MITSUBISHI ELECTRIC RESEARCH LABORATORIES
http://www.merl.com

Split-Horizon MPC for Coupled Station Keeping, Attitude Control, and Momentum Management of GEO Satellites using Electric Propulsion

Caverly, R.; Di Cairano, S.; Weiss, A.

TR2018-093 July 13, 2018

Abstract

In this paper, a model predictive control (MPC) policy is developed to simultaneously perform station keeping, attitude control, and momentum management of a nadirpointing geostationary satellite equipped with three reaction wheels and four on-off electric thrusters mounted on two boom assemblies attached to the anti-nadir face of the satellite. The MPC policy includes an inner-loop SO(3)-based attitude control law to maintain a nadir-pointing attitude, and an outer loop for station keeping and momentum management. The MPC formulation makes use of two different prediction horizons; a short horizon is used for the states associated with the orbit's inclination and a longer horizon is used for all other states. This split-prediction horizon MPC policy leads to a significant reduction in delta-v compared to a single horizon. The continuous thrust command generated by the MPC policy is quantized as a single on-off pulse every feedback period in such a way that the predicted error in the states induced by quantization is minimized, which reduces the number of onoff pulses compared to other quantization approaches in the literature, including pulse-width modulation.

American Control Conference

Split-Horizon MPC for Coupled Station Keeping, Attitude Control, and Momentum Management of GEO Satellites using Electric Propulsion

Ryan J. Caverly[1], Stefano Di Cairano[2], and Avishai Weiss[2]

***Abstract*— In this paper, a model predictive control (MPC) policy is developed to simultaneously perform station keeping, attitude control, and momentum management of a nadir-pointing geostationary satellite equipped with three reaction wheels and four on-off electric thrusters mounted on two boom assemblies attached to the anti-nadir face of the satellite. The MPC policy includes an inner-loop $SO(3)$-based attitude control law to maintain a nadir-pointing attitude, and an outer loop for station keeping and momentum management. The MPC formulation makes use of two different prediction horizons; a short horizon is used for the states associated with the orbit's inclination and a longer horizon is used for all other states. This split-prediction horizon MPC policy leads to a significant reduction in delta-v compared to a single horizon. The continuous thrust command generated by the MPC policy is quantized as a single on-off pulse every feedback period in such a way that the predicted error in the states induced by quantization is minimized, which reduces the number of on-off pulses compared to other quantization approaches in the literature, including pulse-width modulation.**

I. Introduction

Low-thrust electric propulsion is a promising technology that has garnered significant interest within the aerospace community and is increasingly being adopted as the propulsion method of choice for satellites. Electric propulsion has a high specific impulse compared to traditional chemical propulsion, meaning that the same thrust levels can be achieved with less propellant mass [1, Ch. 1]. However, typical electric propulsion systems can only produce a fraction of the thrust of chemical propulsion systems.

In a geostationary Earth orbit (GEO), the magnitude of the perturbation forces acting on the satellite are approximately the same magnitude as the thrust capabilities of an electric propulsion system [2]. Hence, for station keeping applications in GEO, near-continuous operation of the electric propulsion system is required to counteract perturbation-induced drift. As a result, classical station keeping control techniques are impractical with electric propulsion, and a number of novel autonomous feedback control strategies have been proposed specifically for electric propulsion [3–13]. In particular, model predictive control (MPC) policies for simultaneous station keeping, attitude control, and momentum management are promising [11–13], as these critical tasks are often addressed separately in a suboptimal manner.

[1] R. J. Caverly is with the Department of Aerospace Engineering, University of Michigan, Ann Arbor, MI 48109, USA. Email: caverly@umich.edu. He was an intern at MERL during the development of this work.

[2] S. Di Cairano and A. Weiss are with Mitsubishi Research Laboratories, Cambridge, MA 02139, USA. Emails: {dicairano,weiss}@merl.com.

Many electric propulsion systems are not capable of throttling thrust and only operate with on-off pulses. The work of [13] introduced a pulse-width modulation (PWM) scheme to quantize the continuous thrust commanded by an MPC policy as physically realistic on-off commands. This was done by matching the average quantized thrust with the continuous thrust commanded by MPC with roughly 30 pulses per thruster per orbit. In practice, this many pulses would result in a short electric thruster life span due to wear. Other quantization schemes exist in the literature to deal with the on-off nature of electric thrusters [3–8]. The approach used in [3] involves solving a mixed-integer linear program (MILP), which is computationally expensive and difficult to implement in real time, especially on a spacecraft computing platform. PWM schemes are used in [4–6], which present the same issue of many on-off thruster pulses as in [13].

In this paper, the number of on-off thruster pulses is reduced by implementing a single-pulse quantization scheme every time step. A single on-off thrust pulse is made possible by minimizing the predicted state error induced by quantization when solving for the on and off thrust switching times. In an effort to further reduce Δv from [13], a split-horizon MPC policy is also proposed in this paper, which uses a shorter prediction horizon for the states associated with the orbit's inclination. The remainder of the paper proceeds as follows. Section II includes the problem statement and a description of the satellite model. Section III describes the proposed MPC formulation, including the inner-loop attitude controller, the closed-loop linearized satellite model, the split-horizon MPC policy, and the single-pulse thruster quantization scheme. Simulation results are presented in Section IV and closing remarks are given in Section V.

A. Preliminaries and Notation

The following notation will be used throughout the paper. A reference frame $\mathcal{F}_a$ is defined by a set of three orthonormal dextral basis vectors, $\{\underrightarrow{a}^1, \underrightarrow{a}^2, \underrightarrow{a}^3\}$. An arbitrary physical vector, denoted as $\underrightarrow{v}$, is resolved in $\mathcal{F}_a$ as $\mathbf{v}_a$, where $\mathbf{v}_a^{\mathsf{T}} = \begin{bmatrix} v_{a1} & v_{a2} & v_{a3} \end{bmatrix}$ and $\underrightarrow{v} = v_{a1}\underrightarrow{a}^1 + v_{a2}\underrightarrow{a}^2 + v_{a3}\underrightarrow{a}^3$. The mapping between a physical vector resolved in different reference frames is given by the direction cosine matrix (DCM) $\mathbf{C}_{ba} \in SO(3)$, where $SO(3) = \{\mathbf{C} \in \mathbb{R}^{3\times 3} \,|\, \mathbf{C}^{\mathsf{T}}\mathbf{C} = \mathbf{1}, \det(\mathbf{C}) = +1\}$ and $\mathbf{1}$ is the identity matrix. For example, $\mathbf{v}_b = \mathbf{C}_{ba}\mathbf{v}_a$, where $\mathbf{v}_b$ is $\underrightarrow{v}$ resolved in $\mathcal{F}_b$ and $\mathbf{C}_{ba}$ represents the attitude of $\mathcal{F}_b$ relative to $\mathcal{F}_a$. Principle rotations about the $\underrightarrow{a}^i$ axis by an angle α are denoted as $\mathbf{C}_{ba} = \mathbf{C}_i(\alpha)$. The anti-symmetric projection operator $\mathcal{P}_a(\cdot) : \mathbb{R}^{3\times 3} \to \mathfrak{so}(3)$, is given by $\mathcal{P}_a(\mathbf{U}) = \frac{1}{2}\left(\mathbf{U} - \mathbf{U}^{\mathsf{T}}\right)$,

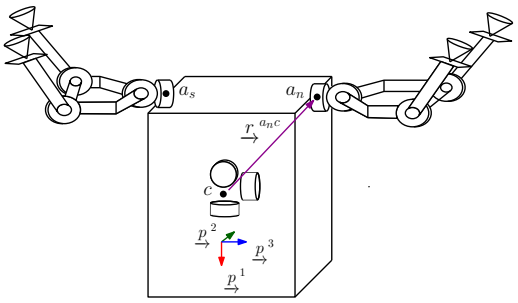

(a)

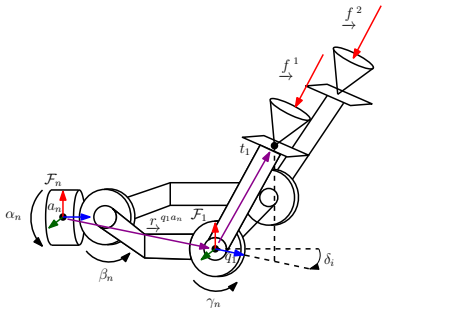

(b)

Fig. 1. Schematic adopted from [13] of the (a) spacecraft including three axisymmetric reaction wheels and four electric thrusters, and (b) North-facing boom-thruster assembly. The first, second, and third axes of each reference frame are respectively denoted by red, green, and blue vectors.

for all $\mathbf{U} \in \mathbb{R}^{3\times3}$, where $\mathfrak{so}(3) = \{\mathbf{S} \in \mathbb{R}^{3\times3} \,|\, \mathbf{S} + \mathbf{S}^\mathsf{T} = \mathbf{0}\}$. The cross operator, $(\cdot)^\times : \mathbb{R}^3 \to \mathfrak{so}(3)$, is defined as

$$\mathbf{a}^\times = -\mathbf{a}^{\times^\mathsf{T}} = \begin{bmatrix} 0 & -a_3 & a_2 \\ a_3 & 0 & -a_1 \\ -a_2 & a_1 & 0 \end{bmatrix},$$

where $\mathbf{a}^\mathsf{T} = \begin{bmatrix} a_1 & a_2 & a_3 \end{bmatrix}$. The uncross operator, $(\cdot)^\vee : \mathfrak{so}(3) \to \mathbb{R}^3$, is defined as $\mathbf{A}^\vee = \begin{bmatrix} a_1 & a_2 & a_3 \end{bmatrix}^\mathsf{T}$, where $\mathbf{A} = \mathbf{a}^\times$. The physical vector describing the position of a point p relative to a point q is given by $\underrightarrow{r}^{pq}$. Similarly, the angular velocity of $\mathcal{F}_b$ relative to $\mathcal{F}_a$ is given by $\underrightarrow{\omega}^{ba}$.

II. Problem Statement and Spacecraft Model

Consider the satellite shown in Fig. 1, which consists of a rigid bus equipped with three axisymmetric reaction wheels and four electric thrusters mounted on gimbaled booms. The satellite is nominally in a circular GEO orbit. The objectives are to 1) minimize fuel consumption (Δv) and 2) limit the number of on-off thruster pulses, while ensuring that

a) the satellite remains within the station-keeping window,
b) angular momentum of the reaction wheels is unloaded,
c) a nadir-pointing attitude is maintained, and
d) the limitations of the thrusters (e.g., thrust magnitude, boom gimbal angle limits) are enforced.

Previous work [11–13] attempted to minimize fuel consumption while satisfying the constraints of a) through d) using MPC policies. An MPC policy is also adopted in this paper, with novel features designed to specifically improve Δv and the number of thruster pulses compared to [11–13].

The satellite model considered in this paper is shown in Fig. 1 and is based on [13]. The Earth-centered inertial (ECI) frame is defined as $\mathcal{F}_g$. The reference frame $\mathcal{F}_p$ is aligned with the spacecraft bus, where nominally $\underrightarrow{p}^1$ points towards the Earth and $\underrightarrow{p}^2$ points North. The angular velocity of $\mathcal{F}_p$ relative to $\mathcal{F}_g$ is $\underrightarrow{\omega}^{pg}$ and the DCM describing the attitude of the spacecraft (i.e., $\mathcal{F}_p$) relative to $\mathcal{F}_g$ is $\mathbf{C}_{pg}$. The center of mass of the spacecraft is denoted by point c in Fig. 1(a). The position of the spacecraft center of mass relative to a point w at the center of the Earth is given by $\underrightarrow{r}^{cw}$. The equations of motion of the satellite are given by [13]

$$\ddot{\mathbf{r}}_g^{cw} = -\mu \frac{\mathbf{r}_g^{cw}}{\left\|\mathbf{r}_g^{cw}\right\|^3} + \mathbf{a}_g^p + \frac{1}{m_\mathcal{B}} \mathbf{C}_{pg}^\mathsf{T} \mathbf{f}_p^{\text{thrust}}, \tag{1a}$$

$$\mathbf{J}_p^{\mathcal{B}c} \dot{\boldsymbol{\omega}}_p^{pg} = -\boldsymbol{\omega}_p^{pg^\times} \left(\mathbf{J}_p^{\mathcal{B}c} \boldsymbol{\omega}_p^{pg} + \mathbf{J}_s \dot{\boldsymbol{\gamma}}\right) - \mathbf{J}_s \boldsymbol{\eta} + \boldsymbol{\tau}_p^p + \boldsymbol{\tau}_p^{\text{thrust}}, \tag{1b}$$

$$\dot{\mathbf{C}}_{pg} = -\boldsymbol{\omega}_p^{pg^\times} \mathbf{C}_{pg}, \tag{1c}$$

$$\ddot{\boldsymbol{\gamma}} = \boldsymbol{\eta}, \tag{1d}$$

where $m_\mathcal{B}$ is the mass of the spacecraft, $\mathbf{J}_p^{\mathcal{B}c}$ is the moment of inertia of the spacecraft relative to point c and resolved in $\mathcal{F}_p$, $\boldsymbol{\gamma}^\mathsf{T} = \begin{bmatrix} \gamma_1 & \gamma_2 & \gamma_3 \end{bmatrix}$ are the reaction wheel angles, $\boldsymbol{\eta}$ is the acceleration of the reaction wheels, $\mathbf{J}_s$ is the moment of inertia of the reaction wheel array, $\mathbf{f}_p^{\text{thrust}}$ is the force produced by the thrusters, $\boldsymbol{\tau}_p^{\text{thrust}}$ is the torque produced by the thrusters, $\mathbf{a}_g^p$ includes acceleration perturbations, and $\boldsymbol{\tau}_p^p$ includes torque perturbations. The thruster configuration is illustrated in Fig. 1, where four electric thrusters are mounted on two boom-thruster assemblies, one of which nominally points North, while the other nominally points South. A detailed view of the North-facing boom-thruster assembly is provided in Fig. 1(b). Each assembly has two fixed gimbal angles, $\bar{\alpha}_a$ and $\bar{\beta}_a$, $a \in \{n, s\}$, as well as an actuated gimbal angle γ_a, $a \in \{n, s\}$. The subscripts n and s refer to the North-facing assembly and the South-facing assembly, respectively. The position of the actuated gimbal of thruster i relative to the spacecraft center of mass is $\underrightarrow{r}^{q_i c}$. The thrusters are canted by fixed angles δ_i, $i = 1, 2, 3, 4$, such that for $\bar{\gamma}_a$, $a \in \{n, s\}$, each thruster fires through the spacecraft center of mass. The force vector produced by thruster i is $\underrightarrow{f}^i$, and can be resolved in $\mathcal{F}_p$ as $\mathbf{f}_p^i = -f^i \mathbf{C}_{ip}^\mathsf{T} \mathbf{C}_2(\gamma_a) \mathbf{1}_3$, where $f^i = \left|\underrightarrow{f}^i\right|$ is the thrust magnitude, $\mathbf{1}_3 = \begin{bmatrix} 0 & 0 & 1 \end{bmatrix}^\mathsf{T}$, $\mathbf{C}_{ip} = \mathbf{C}_{ia}\mathbf{C}_{ap}$, $\mathbf{C}_{ia} = \mathbf{C}_1(\delta_i)\mathbf{C}_2(\bar{\beta}_i)\mathbf{C}_3(\bar{\alpha}_a)$, $\mathbf{C}_{np} = \mathbf{C}_3(\pi)$, and $\mathbf{C}_{sp} = \mathbf{C}_1(\pi)\mathbf{C}_3(\pi)$. The torque generated by the thruster on the spacecraft is given by $\boldsymbol{\tau}_p^i = \mathbf{r}_p^{q_i c^\times} \mathbf{f}_p^i$. The net force and torque applied to the spacecraft by the four thrusters is $\mathbf{f}_p^{\text{thrust}} = \sum_{i=1}^4 \mathbf{B}_i^f \mathbf{u}_i$ and $\boldsymbol{\tau}_p^{\text{thrust}} = \sum_{i=1}^4 \mathbf{B}_i^\tau \mathbf{u}_i$, with $\mathbf{u}_i^\mathsf{T} = \begin{bmatrix} \sin(\gamma_a) f^i & \cos(\gamma_a) f^i \end{bmatrix}$ and constant input matrices $\mathbf{B}_i^f = \mathbf{C}_{ip}^\mathsf{T} \begin{bmatrix} -1 & 0 \\ 0 & 0 \\ 0 & -1 \end{bmatrix}$, $\mathbf{B}_i^\tau = \mathbf{r}_p^{q_i c^\times} \mathbf{B}_i^f$.

For the purposes of station keeping and linearizing the spacecraft's equations of motion, it is useful to express the spacecraft's position relative to the desired nominal circular GEO orbit. To this end, Hill's frame, denoted by $\mathcal{F}_h$, is defined by basis vectors $\underrightarrow{h}^1$ aligned with the orbital radius and $\underrightarrow{h}^3$ orthogonal to the orbital plane. The vector $\underrightarrow{r}^{cw}$ re-

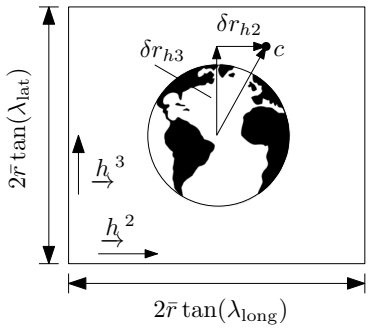

Fig. 2. Illustration of the station keeping window described by $-\bar{r}\tan(\lambda_{\text{long}}) \leq \delta r_{h2} \leq \bar{r}\tan(\lambda_{\text{long}})$ and $-\bar{r}\tan(\lambda_{\text{lat}}) \leq \delta r_{h3} \leq \bar{r}\tan(\lambda_{\text{lat}})$, with the view looking in the $-\hat{h}^1$ direction towards Earth. The point c denotes the spacecraft's center of mass.

solved in $\mathcal{F}_h$ is given by $\mathbf{r}_h^{cw}$. Defining the satellite's nominal position in a circular orbit resolved in $\mathcal{F}_g$ as $\bar{\mathbf{r}}_g$, yields the position error of the spacecraft $\delta\mathbf{r}_h = \begin{bmatrix}\delta r_{h1} & \delta r_{h2} & \delta r_{h3}\end{bmatrix} = \mathbf{r}_h^{cw} - \mathbf{C}_{hg}\bar{\mathbf{r}}_g$. The station keeping window, shown in Fig. 2, is defined as $-\bar{r}\tan(\lambda_{\text{long}}) \leq \delta r_{h2} \leq \bar{r}\tan(\lambda_{\text{long}})$ and $-\bar{r}\tan(\lambda_{\text{lat}}) \leq \delta r_{h3} \leq \bar{r}\tan(\lambda_{\text{lat}})$ [14, Ch. 5], where $\bar{r} = \|\bar{\mathbf{r}}_g\|$, and λ_{long} and λ_{lat} are the maximum deviations in longitude and latitude, respectively. Although no single component of $\delta\mathbf{r}_h$ exactly captures the inclination of the satellite's orbit relative to the desired circular orbit, for small deviations from the center of the station keeping window the coordinate δr_{h3} approximates this inclination. This approximation is relevant in the split-horizon MPC policy of Section III-D, where the states δr_{h3}^{cw} and $\delta\dot{r}_{h3}^{cw}$ use a different prediction horizon than the rest of the system states.

III. MPC Formulation

The novel contributions of this work compared to [11–13] include a split-horizon MPC policy to reduce Δv, and a single-pulse thruster quantization scheme that minimizes the predicted state error induced by quantization, which leads to a reduction in the number of thruster on-off pulses.

A. Inner-Loop Attitude Controller

The reaction wheels are directly actuated by the spacecraft attitude controller, which is seen as an inner-loop controller by the MPC policy. The disturbance torque is assumed to be described by the LTI system $\dot{\mathbf{x}}_{\text{dist}} = \mathbf{A}_{\text{dist}}\mathbf{x}_{\text{dist}}$, $\boldsymbol{\tau}_p^p = \mathbf{C}_{\text{dist}}\mathbf{x}_{\text{dist}}$. An observer is designed to estimate the disturbance using the form $\dot{\hat{\mathbf{x}}}_{\text{dist}} = \mathbf{A}_{\text{dist}}\hat{\mathbf{x}}_{\text{dist}} + \mathbf{B}_{\text{dist}}\mathbf{u}_{\text{dist}}$ and $\hat{\boldsymbol{\tau}}_p^p = \mathbf{C}_{\text{dist}}\hat{\mathbf{x}}_{\text{dist}}$, where $\hat{\boldsymbol{\tau}}_p^p$ is the estimate of $\boldsymbol{\tau}_p^p$, $\mathbf{u}_{\text{dist}} = \boldsymbol{\omega}_p^{pd} + \mathbf{K}_1\mathbf{S}$, $\mathbf{K}_1 = \mathbf{K}_1^{\mathsf{T}} > 0$, and $\mathbf{S} = -\boldsymbol{\mathcal{P}}_a\left(\mathbf{C}_{pd}\right)^{\vee}$. The matrix $\mathbf{B}_{\text{dist}} = \mathbf{P}_{\text{dist}}^{-1}\mathbf{C}_{\text{dist}}^{\mathsf{T}}$ is designed such that $(\mathbf{A}_{\text{dist}}, \mathbf{B}_{\text{dist}}, \mathbf{C}_{\text{dist}})$ is positive real, where $\mathbf{P}_{\text{dist}} = \mathbf{P}_{\text{dist}}^{\mathsf{T}} > 0$ satisfies the Lyapunov equation $\mathbf{A}_{\text{dist}}^{\mathsf{T}}\mathbf{P}_{\text{dist}} + \mathbf{P}_{\text{dist}}\mathbf{A}_{\text{dist}} = -\mathbf{Q}_{\text{dist}}$ with $\mathbf{Q}_{\text{dist}} = \mathbf{Q}_{\text{dist}}^{\mathsf{T}} \geq 0$ [15, p. 218]. The attitude controller is adapted from [16] as

$$
\begin{aligned}
\boldsymbol{\nu}_1 &= \boldsymbol{\omega}_p^{\times}\left(\mathbf{J}_p^{\mathcal{B}c}\boldsymbol{\omega}_p + \mathbf{J}_s\dot{\boldsymbol{\gamma}}\right) - \mathbf{J}_p^{\mathcal{B}c}\left(\mathbf{K}_1\dot{\mathbf{S}} + \boldsymbol{\omega}_p^{pd\times}\boldsymbol{\omega}_p\right),\\
\boldsymbol{\nu}_2 &= -\hat{\boldsymbol{\tau}}_p^p,\\
\boldsymbol{\nu}_3 &= -\mathbf{K}_{\nu}\left(\boldsymbol{\omega}_p^{pd} + \mathbf{K}_1\mathbf{S}\right) - \mathbf{K}_p\mathbf{S},
\end{aligned}
$$

where $\mathbf{K}_{\nu} = \mathbf{K}_{\nu}^{\mathsf{T}} > 0$, $\mathbf{K}_p = \mathbf{K}_p^{\mathsf{T}} > 0$, and the attitude control input is $\boldsymbol{\eta} = -\mathbf{J}_s^{-1}\left(\boldsymbol{\nu}_1 + \boldsymbol{\nu}_2 + \boldsymbol{\nu}_3\right)$.

B. Closed-Loop Linearized Model

The MPC prediction model is obtained by linearizing the spacecraft dynamics in closed-loop with the attitude controller about a nominal circular orbit with mean motion n, a nadir-pointing attitude, zero reaction wheel speeds, and zero observer states, and is given by [12], [13]

$$
\begin{aligned}
\delta\ddot{\mathbf{r}}_h &= -2\bar{\boldsymbol{\omega}}_p^{\times}\delta\dot{\mathbf{r}}_h - \boldsymbol{\Omega}\delta\mathbf{r}_h + \mathbf{a}_h^p + \frac{1}{m_{\mathcal{B}}}\mathbf{C}_{dh}^{\mathsf{T}}\mathbf{f}_p^{\text{thrust}},\\
\delta\dot{\boldsymbol{\omega}} &= \left(\mathbf{K}_1\bar{\boldsymbol{\omega}}_p^{\times} - \left(\bar{\boldsymbol{\omega}}_p^{\times}\right)^2 + \mathbf{J}_p^{\mathcal{B}c^{-1}}\left(\mathbf{K}_{\nu}\bar{\boldsymbol{\omega}}_p^{\times} - \mathbf{K}\right)\right)\delta\boldsymbol{\theta} + \boldsymbol{\tau}_p^{\text{thrust}}\\
&\quad + \left(-\mathbf{K}_1 + \bar{\boldsymbol{\omega}}_p^{\times} - \mathbf{J}_p^{\mathcal{B}c}\mathbf{K}_{\nu}\right)\delta\boldsymbol{\omega} - \mathbf{J}_p^{\mathcal{B}c^{-1}}\mathbf{C}_{\text{dist}}\tilde{\mathbf{x}}_{\text{dist}},\\
\ddot{\boldsymbol{\gamma}} &= \boldsymbol{\eta},\\
\dot{\tilde{\mathbf{x}}} &= \mathbf{A}_{\text{dist}}\tilde{\mathbf{x}}_{\text{dist}} + \mathbf{B}_{\text{dist}}\delta\boldsymbol{\omega} + \mathbf{B}_{\text{dist}}\left(\mathbf{K}_1 - \bar{\boldsymbol{\omega}}_p^{\times}\right)\delta\boldsymbol{\theta},
\end{aligned}
$$

where $\bar{\boldsymbol{\omega}}_p^{\mathsf{T}} = \begin{bmatrix}0 & 0 & n\end{bmatrix}$, $\mathbf{C}_{pd} = \mathbf{C}_{pg}\mathbf{C}_{dg}^{\mathsf{T}}$ is the attitude error between $\mathbf{C}_{pg}$ and the desired nadir-pointing orientation $\mathbf{C}_{dg}$, $\mathbf{C}_{pg}$ is parameterized by a $3-2-1$ Euler angle sequence with angles $\delta\boldsymbol{\theta}^{\mathsf{T}} = \begin{bmatrix}\delta\phi & \delta\theta & \delta\psi\end{bmatrix}$, $\mathbf{K} = \mathbf{K}_{\nu}\mathbf{K}_1 + \mathbf{K}_p$, and $\boldsymbol{\Omega} = \text{diag}\{-3n^2, 0, n^2\}$. See [12], [13] for further details on this linearization. The closed-loop linearized model is written in state-space form as $\dot{\mathbf{x}} = \mathbf{A}\mathbf{x} + \mathbf{B}\mathbf{u} + \mathbf{B}_w\mathbf{w}$, where $\mathbf{x}^{\mathsf{T}} = \begin{bmatrix}\delta\mathbf{r}^{\mathsf{T}} & \delta\dot{\mathbf{r}}^{\mathsf{T}} & \delta\boldsymbol{\theta}^{\mathsf{T}} & \delta\boldsymbol{\omega}^{\mathsf{T}} & \dot{\boldsymbol{\gamma}}^{\mathsf{T}} & \tilde{\mathbf{x}}_{\text{dist}}^{\mathsf{T}}\end{bmatrix}$, $\mathbf{u}^{\mathsf{T}} = \begin{bmatrix}\mathbf{u}_1^{\mathsf{T}} & \mathbf{u}_2^{\mathsf{T}} & \mathbf{u}_3^{\mathsf{T}} & \mathbf{u}_4^{\mathsf{T}}\end{bmatrix}$, and $\mathbf{w} = \mathbf{a}_h^p$. The discrete-time model with time step Δt is $\mathbf{x}_{k+1} = \mathbf{A}_{\text{d}}\mathbf{x}_k + \mathbf{B}_{\text{d}}\mathbf{u}_k + \mathbf{B}_{w,\text{d}}\mathbf{w}_k$.

C. MPC Input and State Constraints

The magnitude of each thruster must satisfy $\left\|\mathbf{f}_i^i\right\|_2 \leq f_{\text{max}}$, where f_{max} is the maximum allowable thrust. To simplify the MPC formulation, this quadratic constraint is approximated by the linear constraint $\left\|\mathbf{f}_i^i\right\|_1 \leq f_{\text{max}}$. It is also imperative that the thrusters fire away from the spacecraft bus, which is enforced by the constraint $\mathbf{f}_i^i \leq 0$. The control constraints are $\mathbf{u}_{\text{min}} \leq \mathbf{u}_i \leq \mathbf{u}_{\text{max}}$, $i = 1, 2, 3, 4$, where $\mathbf{u}_{\text{max}^{\mathsf{T}}} = f_{\text{max}}\begin{bmatrix}1 & 1\end{bmatrix}$ and $\mathbf{u}_{\text{min}} = \mathbf{0}$. There is an additional physical constraint that the gimbal angle γ_n must be identical for the pair of inputs $\mathbf{u}_1$ and $\mathbf{u}_2$ at any time instant, since they share this angle. The same is true for γ_s with the pair of inputs $\mathbf{u}_3$ and $\mathbf{u}_4$. As in [13], this constraint is ignored in the MPC policy and is addressed in the quantization scheme.

The two state constraints considered in this policy are based on the prescribed station keeping window and the maximum allowable attitude error. Since the closed-loop linearized orbital dynamics equation of motion is given in Hill's frame, the station keeping window constraint can be written as $\delta\bar{\mathbf{r}}_{\text{min}} \leq \delta\bar{\mathbf{r}} \leq \delta\bar{\mathbf{r}}_{\text{max}}$, where $\delta\bar{\mathbf{r}}_{\text{max}}^{\mathsf{T}} = \begin{bmatrix}\infty & \bar{r}\tan(\lambda_{\text{long}}) & \bar{r}\tan(\lambda_{\text{lat}})\end{bmatrix}$, and $\delta\bar{\mathbf{r}}_{\text{min}} = -\delta\bar{\mathbf{r}}_{\text{max}}$. The constraint on attitude error is written as $\delta\boldsymbol{\theta}_{\text{min}} \leq \delta\boldsymbol{\theta} \leq \delta\boldsymbol{\theta}_{\text{max}}$.

D. Split-Horizon MPC Policy

Consider the split-horizon MPC policy stated as

$$
\begin{aligned}
\min_{\mathcal{U}_t}\ & \mathbf{x}_{N_1|t}^{\mathsf{T}}\mathbf{P}_1\mathbf{x}_{N_1|t} + \sum_{k=0}^{N_1-1}\left(\mathbf{x}_{k|t}^{\mathsf{T}}\mathbf{Q}\mathbf{x}_{k|t} + \mathbf{u}_{k|t}^{\mathsf{T}}\mathbf{R}\mathbf{u}_{k|t}\right)\\
&+ \mathbf{x}_{N_2|t}^{\mathsf{T}}\mathbf{P}_2\mathbf{x}_{N_2|t} + \sum_{k=N_1}^{N_2-1}\left(\mathbf{x}_{k|t}^{\mathsf{T}}\mathbf{Q}_2\mathbf{x}_{k|t} + \mathbf{u}_{k|t}^{\mathsf{T}}\mathbf{R}\mathbf{u}_{k|t}\right), \quad (2)
\end{aligned}
$$

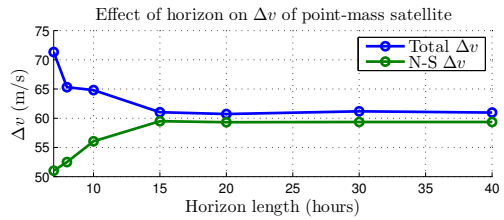

(a)

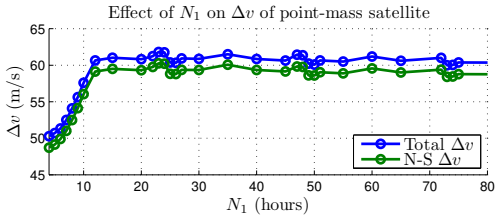

(b)

Fig. 3. Plots of annual Δv with a point-mass satellite and a $\pm 0.01^\circ$ station keeping window for varying (a) $N_1 = N_2$ and (b) N_1 with $N_2 = 15$ hours.

subject to $\mathbf{x}_{k+1|t} = \mathbf{A}_\mathrm{d}\mathbf{x}_{k|t} + \mathbf{B}_\mathrm{d}\mathbf{u}_{k|t} + \mathbf{B}_{w,\mathrm{d}}\mathbf{w}_{k|t}$, $\mathbf{x}_{0|t} = \mathbf{x}(t)$, $\mathbf{w}_{k|t} = \hat{\mathbf{w}}_t(t+k)$, $\mathbf{x}_\mathrm{min} \leq \mathbf{x}_{k|t} \leq \mathbf{x}_\mathrm{max}$ for $0 \leq k \leq N_1$, $\mathbf{x}_{\mathrm{min},2} \leq \mathbf{x}_{k|t} \leq \mathbf{x}_{\mathrm{max},2}$ for $N_1 < k \leq N_2$, and $\mathbf{u}_\mathrm{min} \leq \mathbf{u}_{k|t} \leq \mathbf{u}_\mathrm{max}$, where N_1 is the prediction horizon of the states δr_{h3}^{cw} and $\delta \dot{r}_{h3}^{cw}$, N_2 is the prediction horizon of the remaining states, $\mathcal{U}_t = \{\mathbf{u}_{0|t}, \ldots, \mathbf{u}_{N_2-1|t}\}$, $\mathbf{Q} = \mathbf{Q}^\mathsf{T} \geq 0$ and $\mathbf{R} = \mathbf{R}^\mathsf{T} > 0$ are constant state and control weighting matrices, and $\hat{\mathbf{w}}_i(j)$ is the open-loop predicted disturbance column matrix at time j based on data at time i. The matrix $\mathbf{Q}_2$ is the same as $\mathbf{Q}$, except the rows and columns associated with the states δr_{h3}^{cw} and $\delta \dot{r}_{h3}^{cw}$ are set to zero. The matrices $\mathbf{P}_1$ and $\mathbf{P}_2$ are constructed from the matrix $\mathbf{P} = \mathbf{P}^\mathsf{T} > 0$, which is the solution to the Discrete Algebraic Riccati Equation (DARE). The matrix $\mathbf{P}_1$ contains the rows and columns of $\mathbf{P}$ associated with the states δr_{h3}^{cw} and $\delta \dot{r}_{h3}^{cw}$ and zeros the others, while $\mathbf{P}_2$ does the opposite, so that $\mathbf{P}_1 + \mathbf{P}_2 = \mathbf{P}$. This is possible since $\mathbf{P}$ is block-diagonal under a coordinate transformation that reorders the states such that δr_{h3}^{cw} and $\delta \dot{r}_{h3}^{cw}$ are at the end of the state column matrix. The state constraints $\mathbf{x}_\mathrm{min}$ and $\mathbf{x}_\mathrm{max}$ are based on the station keeping and attitude constraints. The state constraints $\mathbf{x}_{\mathrm{min},2}$ and $\mathbf{x}_{\mathrm{max},2}$ are identical to $\mathbf{x}_\mathrm{min}$ and $\mathbf{x}_\mathrm{max}$, except $\delta\mathbf{r}_\mathrm{min}^\mathsf{T} = \begin{bmatrix} -\infty & -\bar{r}\tan(\lambda_\mathrm{long}) & -\infty \end{bmatrix}$ and $\delta\mathbf{r}_\mathrm{max}^\mathsf{T} = \begin{bmatrix} \infty & \bar{r}\tan(\lambda_\mathrm{long}) & \infty \end{bmatrix}$ are used. The control input is selected as $\mathbf{u}(t) = \mathbf{u}_{0|t}^*$, where $\mathbf{u}_{0|t}^*$ is the first element of $\mathcal{U}_t^*$, the minimizer of (2).

The motivation for developing a split-horizon MPC policy came from a study on the effect of the prediction horizon on the yearly Δv required to keep a point-mass satellite equipped with 12 electric thrusters and orbital dynamics described by (1a) within a $\pm 0.01^\circ$ station keeping window. A plot of the yearly Δv for a non-split prediction horizon ($N_1 = N_2$) ranging from 5 hours to 40 hours is shown in Fig. 3(a), where $\Delta t = 1$ hour. The total Δv clearly increases with decreasing horizon, however, it is observed that the North-South (N-S) component of Δv *decreases* with decreasing horizon. This decrease in N-S Δv is masked in the total Δv by a larger increase in East-West (E-W) Δv with decreasing horizon. This unexpected behavior inspired the use of a split prediction horizon MPC policy. The plot of Fig. 3(b) is very similar to the plot of Fig. 3(a), but only the prediction horizon N_1 is varied while $N_2 = 15$ hours is held constant. This plot shows that both the total Δv and the N-S Δv decrease with decreasing N_1 under 12 hours. The total Δv and the N-S Δv also decrease with increasing N_1 over 12 hours, however, this decrease is minimal for N_1 of less than a few days. It is postulated that the decrease in Δv observed with shorter N_1 is due to the choice of coordinates used to represent the orbital dynamics. In particular, the state δr_{h3}^{cw} is an approximation of the orbit's inclination, and over a full orbit with a constant non-zero inclination, δr_{h3}^{cw} will be positive for half the orbit and negative for the other half. A long prediction horizon will include this oscillatory behavior in δr_{h3}^{cw}, and the MPC policy may not attempt to correct a deviation in δr_{h3}^{cw} at the current time step. By not correcting for deviations in δr_{h3}^{cw} early enough, the satellite's orbit will remain inclined and most likely additional fuel will be required in subsequent time steps, as the satellite approaches the edges of the station keeping window. A shorter prediction horizon will not include as much of this oscillatory behavior, and will correct deviations in δr_{h3}^{cw} earlier, which has been shown to result in less annual Δv. It is possible that a model with orbital elements as states will not feature a decrease in Δv with shorter prediction horizon, which will be topic of future research.

E. Thruster Quantization

The low-thrust electric thrusters of the spacecraft are operated with on-off pulses. The control input generated by the MPC policy in Section III-D is a continuous thrust value for each thruster, which cannot be used directly with the thrusters. As such, the control input is quantized to on-off pulses. A PWM quantization scheme was developed in [13] with a fixed frequency of five on-off pulses per time step with varying pulse widths, which works well, but leads to approximately 30 pulses per thruster per orbit. In an effort to reduce the number of on-off pulses, a single pulse quantization scheme is proposed in this section.

As shown in Figure 4, consider the quantization of a piecewise constant control input sequence, $\mathbf{u}_\mathrm{mpc}$, over a time step beginning at time t_0 and ending at time $t_f = t_0 + \Delta t$, where only a single pulse of magnitude f_max is applied at the i^th thruster starting at time $t_{1,i}$ and ending at time $t_{2,i}$, where $t_0 \leq t_{1,i} < t_{2,i} \leq t_f$. The quantization is executed by minimizing a function of the error between the predicted states of the system at time t_f using the piecewise constant MPC input sequence $\mathbf{u}_\mathrm{mpc}$ and the predicted states at t_f using a single pulse quantized input for each thruster, subject to constraints on the thrusters' operation. The predicted states of the system at time t_f with the quantized thrust inputs are given by $\mathbf{x}_\mathrm{quant}(t_f) = e^{\mathbf{A}\Delta t}\mathbf{x}(t_0) + \sum_{i=1}^{4} e^{\mathbf{A}(t_f - t_{2,i})}\mathbf{B}_{d,i}(t_{1,i}, t_{2,i})\mathbf{u}_{\mathrm{max},i}$, where

$$\mathbf{u}_{\mathrm{max},i} = \begin{cases} f_\mathrm{max}\dfrac{\mathbf{u}_{\mathrm{mpc},0|t_0,i}}{\left\|\mathbf{u}_{\mathrm{mpc},0|t_0,i}\right\|} & \left\|\mathbf{u}_{\mathrm{mpc},0|t_0,i}\right\| \geq \epsilon \\ \mathbf{0} & \left\|\mathbf{u}_{\mathrm{mpc},0|t_0,i}\right\| < \epsilon \end{cases},$$

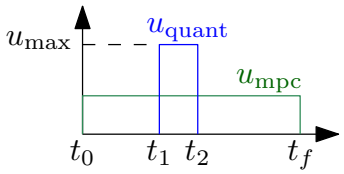

Fig. 4. Single quantized on-off thrust pulse (u_{quant}) over one time step for a given thruster.

$\mathbf{u}_{\text{mpc},0|t_0}^{\mathsf{T}} = \begin{bmatrix}\mathbf{u}_{\text{mpc},0|t_0,1}^{\mathsf{T}} & \mathbf{u}_{\text{mpc},0|t_0,2}^{\mathsf{T}} & \mathbf{u}_{\text{mpc},0|t_0,3}^{\mathsf{T}} & \mathbf{u}_{\text{mpc},0|t_0,4}^{\mathsf{T}}\end{bmatrix}$ is the MPC input, and $\epsilon > 0$ is the tolerance below which the MPC input is considered to be zero. The predicted states of the system with the MPC inputs can be expressed as $\mathbf{x}_{\text{mpc}}(t_f) = e^{\mathbf{A}\Delta t}\mathbf{x}(t_0) + \mathbf{A}_{\text{d}}\mathbf{u}_{\text{mpc},0|t_0}$, where $\mathbf{B}_{\text{d}} = \int_0^{\Delta t} e^{\mathbf{A}(\Delta t-\tau)}\text{d}\tau\mathbf{B}$ is the discrete-time $\mathbf{B}$ matrix calculated with time step Δt. The error between the two predicted states at t_f is given by $\mathbf{e} = \mathbf{x}_{\text{mpc}}(t_f) - \mathbf{x}_{\text{quant}}(t_f) = \mathbf{A}_{\text{d}}\mathbf{u}_{\text{mpc},0|t_0} - \sum_{i=1}^{4} e^{\mathbf{A}(t_f-t_{2,i})}\mathbf{B}_{d,i}(t_{1,i},t_{2,i})\mathbf{u}_{\max,i}$. The switching times for each thruster must satisfy $t_0 \le t_{1,i} < t_{2,i} \le t_f$, $i = 1,2,3,4$. Additionally, more than one thruster on the North or South-facing boom-thruster assembly should not fire at the same time, since these thruster share the gimbal angle γ_a, $a \in \{n, s\}$. This results in a constraint on the switching times of the thrusters so that they never overlap. As the firing order of the thrusters may have an impact on the predicted state error, different orders of thruster firings are considered: 1 before 2 and 3 before 4 (Mode 1), as well as 2 before 1 and 4 before 3 (Mode 2). Each mode amounts to a different set of linear inequality constraints on the switching times to prevent overlapping. The cost function is the weighted norm of the error, $J(\mathbf{e}) = \mathbf{e}^{\mathsf{T}}\mathbf{W}\mathbf{e}$, where $\mathbf{W} = \mathbf{W}^{\mathsf{T}} \ge 0$. If no thruster exceeds ϵ during the time step, then all thrust commands are set to zero and no optimization problem is solved. Otherwise, a first set of switching times $t_{1,i}$, $t_{2,i}$, $i = 1,2,3,4$ is solved by minimizing $J(\mathbf{e})$ satisfying Mode 1 constraints and a second set is solved with Mode 2 constraints. The solution that results in a smaller cost function value is used as the optimal solution to the quantization scheme.

IV. Simulation Results

The MPC policy formulated in Section III is implemented in a numerical simulation of the nonlinear spacecraft dynamic model presented in (1), which has been validated using Systems Tool Kit (STK) in [17]. A spacecraft in GEO is considered using the same physical parameters as [13]. The spacecraft has a mass of 4000 kg, and reactions wheels each with a mass of 20 kg, a radius of 0.75 m, and a thickness of 0.2 m. The nominal gimbal angles of the boom-thruster assemblies are $\bar{\alpha}_n = \bar{\alpha}_s = \bar{\beta}_n = \bar{\beta}_s = 0^\circ$ and $\bar{\gamma}_n = \bar{\gamma}_s = 40.14^\circ$. Further details of the boom-thruster assembly physical parameters can be found in [13]. Perturbations due to Earth's oblateness, solar and lunar gravitational attraction, and solar radiation pressure are included in the simulation [11]. Solar radiation pressure is also considered in the calculation of a disturbance torque, as done in [18, p. 229], with the numerical values found in [13]. The performance constraints considered in simulation include a maximum thruster magnitude of 0.1 N, a station keeping window of $\pm 0.05^\circ$ in both latitude and longitude, and a maximum allowable attitude error of $\pm 0.02^\circ$ in yaw, pitch, and roll. Simulations are performed for 425 orbits, but only the results from the last 365 orbits are presented and used for analysis, to remove the initial transient behavior.

A simulation is first performed using the non-quantized MPC policy from [13] to provide a baseline for Δv performance. The MPC policy uses a prediction horizon of 20 hours, a discretization time step of $\Delta t = 1$ hour, and weighting matrices of $\mathbf{Q} = \text{diag}\{\mathbf{Q}_{\mathbf{r}}, \mathbf{Q}_{\dot{\mathbf{r}}}, \mathbf{Q}_{\boldsymbol{\theta}}, \mathbf{Q}_{\boldsymbol{\omega}}, \mathbf{Q}_{\dot{\boldsymbol{\gamma}}}, \mathbf{Q}_{\tilde{\mathbf{x}}_{\text{dist}}}\}$ and $\mathbf{R} = \mathbf{R}_{\text{thrust}} + \mathbf{R}_{\text{torque}}$, where $\mathbf{Q}_{\mathbf{r}} = 10^{-3} \cdot \text{diag}\{0,1,1\}$ 1/m^2, $\mathbf{Q}_{\dot{\mathbf{r}}} = \mathbf{0}$ s^2/m^2, $\mathbf{Q}_{\boldsymbol{\theta}} = 10^{-3} \cdot \mathbf{1}$ 1/rad^2, $\mathbf{Q}_{\boldsymbol{\omega}} = 10^{-3} \cdot \mathbf{1}$ s^2/rad^2, $\mathbf{Q}_{\dot{\boldsymbol{\gamma}}} = 10^{-4} \cdot \mathbf{1}$ s^2/rad^2, $\mathbf{Q}_{\tilde{\mathbf{x}}_{\text{dist}}} = \mathbf{0}$, $\mathbf{R}_{\text{thrust}} = 10^4$ 1/N^2, $\mathbf{R}_{\text{torque}} = 10^4 \cdot \mathbf{L}^{\mathsf{T}}\mathbf{L}$, where $\mathbf{L} = \text{diag}\{\mathbf{B}_1^{\tau}, \mathbf{B}_2^{\tau}, \mathbf{B}_3^{\tau}, \mathbf{B}_4^{\tau}\}$. The inner-loop attitude controller gains are $\mathbf{K}_1 = 0.2 \cdot \mathbf{1}$ 1/s, $\mathbf{K}_p = 2 \cdot \mathbf{1}$ N·m, $\mathbf{K}_\nu = 100 \cdot \mathbf{1}$ N·m·s. The observer dynamics of the inner-loop attitude controller are chosen as $\mathbf{A}_{\text{dist}} = \text{diag}\{\bar{\mathbf{A}}_{\text{dist}}, \bar{\mathbf{A}}_{\text{dist}}, \bar{\mathbf{A}}_{\text{dist}}\}$ and $\mathbf{C}_{\text{dist}} = \text{diag}\{\bar{\mathbf{C}}_{\text{dist}}, \bar{\mathbf{C}}_{\text{dist}}, \bar{\mathbf{C}}_{\text{dist}}\}$, where $\bar{\mathbf{A}}_{\text{dist}} = \begin{bmatrix}-0.001 & -\omega_d^2 \\ 1 & -0.001\end{bmatrix}$, $\omega_d = 2\pi$ rad/day, and $\bar{\mathbf{C}}_{\text{dist}} = \begin{bmatrix}1 & 0\end{bmatrix}$. The observer matrix $\bar{\mathbf{B}}_{\text{dist}}$ is given by $\bar{\mathbf{B}}_{\text{dist}} = \mathbf{P}_{\text{dist}}^{-1}\bar{\mathbf{C}}_{\text{dist}}^{\mathsf{T}}$, where $\mathbf{P}_{\text{dist}} = \mathbf{P}_{\text{dist}}^{\mathsf{T}} \ge 0$ satisfies the Lyapunov equation $\bar{\mathbf{A}}_{\text{dist}}^{\mathsf{T}}\mathbf{P}_{\text{dist}} + \mathbf{P}_{\text{dist}}\bar{\mathbf{A}}_{\text{dist}} = -\mathbf{Q}_{\text{dist}}$ with $\mathbf{Q}_{\text{dist}} = 10^{-3} \cdot \mathbf{1}$. The resulting Δv with the non-quantized MPC policy from [13] is 73.4 m/s. The MPC policy in Section III without the quantization of Section III-E is implemented in the same simulation, with identical controller parameters except with a split prediction horizon where $N_1 = 5$ hours, $N_2 = 20$ hours. This MPC policy yields a Δv of 65.9 m/s, which amounts to roughly a 10% savings compared to the MPC policy from [13]. Another simulation is performed with the quantized MPC policy of Section III with identical control parameters as the previous simulation, a thrust cutoff of $\epsilon = 0.01$ mN, and the weighting matrix $\mathbf{W} = \text{diag}\{\mathbf{W}_{\mathbf{r}}, \mathbf{W}_{\dot{\mathbf{r}}}, \mathbf{W}_{\boldsymbol{\theta}}, \mathbf{W}_{\boldsymbol{\omega}}, \mathbf{W}_{\dot{\boldsymbol{\gamma}}}, \mathbf{W}_{\tilde{\mathbf{x}}_{\text{dist}}}\}$, where $\mathbf{W}_{\mathbf{r}} = 10^{-4} \cdot \text{diag}\{1,1,10^3\}$ 1/m^2, $\mathbf{W}_{\dot{\mathbf{r}}} = \mathbf{1}$ s^2/m^2, $\mathbf{W}_{\boldsymbol{\theta}} = 10^4 \cdot \mathbf{1}$ 1/rad^2, $\mathbf{W}_{\boldsymbol{\omega}} = 10^{-1} \cdot \mathbf{1}$ s^2/rad^2, $\mathbf{W}_{\dot{\boldsymbol{\gamma}}} = 10 \cdot \mathbf{1}$ s^2/rad^2, and $\mathbf{W}_{\tilde{\mathbf{x}}_{\text{dist}}} = 10 \cdot \mathbf{1}$. The results of this simulation are included in Fig. 5, where a Δv of 65.9 m/s is achieved with an average of 2.7 pulses per thruster per orbit. This Δv is the same as without quantization, and the number of thruster pulses is reduced by a factor of ten compared to the PWM scheme in [13]. Figs. 5(a), 5(b), 5(c) show that constraints are satisfied throughout the simulation and momentum management is performed.

V. Conclusions

In this paper it was shown that a split-horizon MPC policy can yield a significant reduction in the Δv required for simultaneous station keeping and momentum management of a GEO satellite compared to a standard non-split horizon MPC policy. A novel single-pulse quantization method was also presented that reduces the number of on-off thruster pulses required for station keeping, without sacrificing performance in Δv. The contributions of this paper led to significant improvements in performance compared to the results

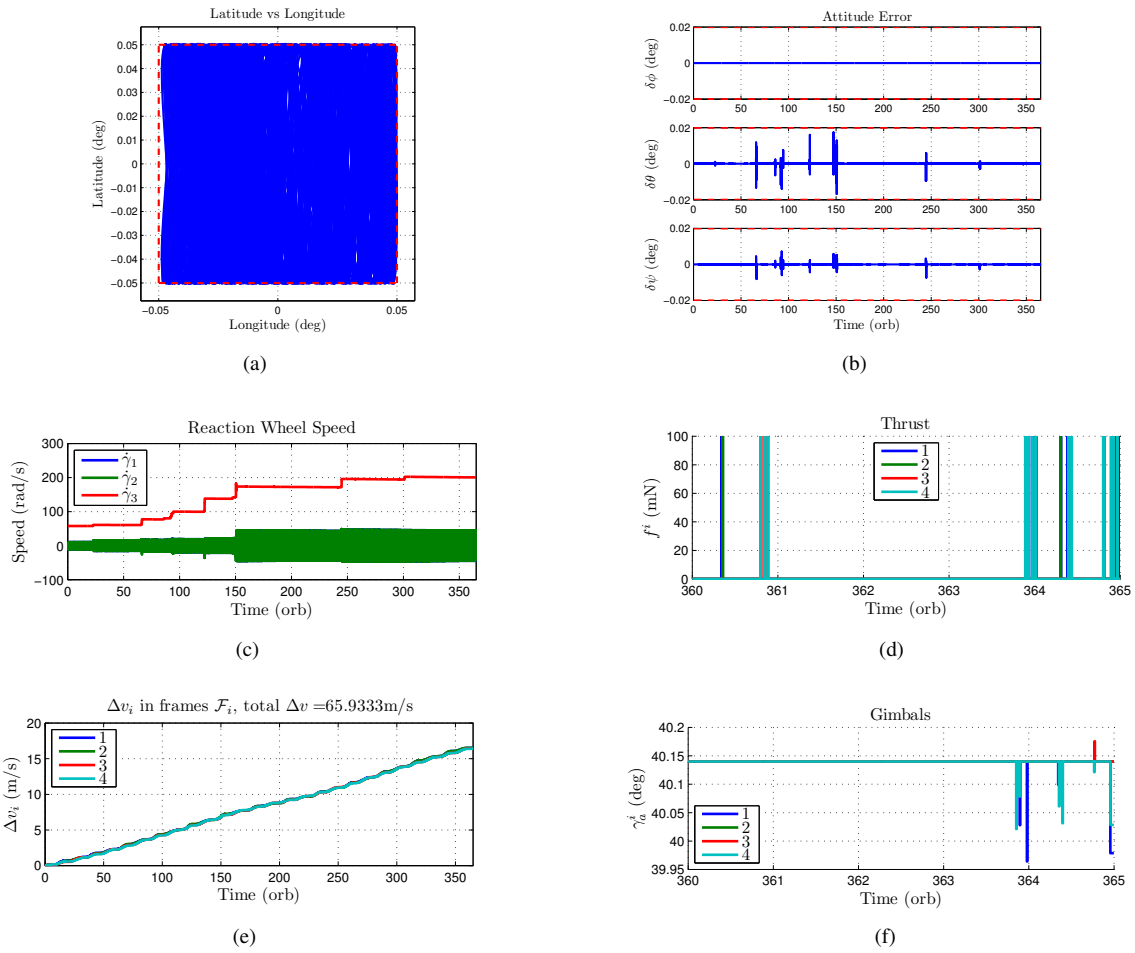

Fig. 5. One year simulation using the quantized MPC policy of Section III. Plots include the (a) station keeping window, (b) spacecraft attitude error, (c) reaction wheel speeds, (d) thrust forces over the last 5 orbits, (e) accumulation of Δv for each thruster, and (f) gimbal angles over the last 5 orbits.

of [13], and yielded a control policy that is realistically implementable on existing flight hardware. Future work will investigate the effect on Δv and the number of thruster pulses of the thruster magnitude cutoff.

REFERENCES

[1] D. M. Goebel and I. Katz, *Fundamentals of Electric Propulsion: Ion and Hall Thrusters*. John Wiley & Sons, 2008, vol. 1.

[2] H. Kuninaka and K. Kajiwara, "Overview of JAXA's activities on electric propulsion," in *P. Int. Elec. Propul. Conf.*, 2011, p. 332.

[3] M. Leomanni, A. Garulli, A. Giannitrapani, and F. Scortecci, "All-electric spacecraft precision pointing using model predictive control," *J. Guid. Control Dynam.*, vol. 38, no. 1, pp. 161–168, 2015.

[4] M. Leomanni, E. Rogers, and S. B. Gabriel, "Explicit model predictive control approach for low-thrust spacecraft proximity operations," *J. Guid. Control Dynam.*, vol. 37, no. 6, pp. 1780–1790, 2014.

[5] R. Vazquez, F. Galivan, and E. F. Camacho, "Pulse-width predictive control for LTV systems with application for spacecraft rendez-vous," *Control Eng. Pract.*, vol. 60, pp. 199–210, 2017.

[6] C. Gazzino, C. Louembet, D. Arzelier, N. Jozefowiez, D. Losa, C. Pittet, and L. Cerri, "Integer programming for optimal control of geostationary station keeping of low-thrust satellites," LAAS Report 16341, July 2017.

[7] C. Gazzino, D. Arzelier, L. Cerri, D. Losa, C. Louembet, and C. Pittet, "Solving the minimum-fuel low-thrust geostationary station keeping problem via the switching systems theory," in *European Conf. Aeronaut. Space Sci.*, July 2017.

[8] C. Gazzino, D. Arzelier, D. Losa, C. Louembet, C. Pittet, and L. Cerri, "Optimal control for minimum-fuel geostationary station keeping of satellites equipped with electric propulsion," *IFAC Papers Online*, vol. 49, no. 17, pp. 379–384, 2016.

[9] Y. Ulybyshev, "Long-term station keeping of space station in lunar halo orbits," *J. Guid. Control Dynam.*, vol. 38, no. 6, pp. 1063–1070, 2014.

[10] A. Garulli, A. Giannitrapani, M. Leomanni, and F. Scortecci, "Autonomous low-earth-orbit station-keeping with electric propulsion," *J. Guid. Control Dynam.*, vol. 34, no. 6, pp. 1683–1693, 2011.

[11] A. Weiss, U. Kalabić, and S. Di Cairano, "Model predictive control for simultaneous station keeping and momentum management of low-thrust satellites," in *P. Amer. Contr. Conf.*, 2015, pp. 2305–2310.

[12] A. Walsh, S. Di Cairano, and A. Weiss, "MPC for coupled station keeping, attitude control, and momentum management of low-thrust geostationary satellites," in *P. Amer. Contr. Conf.*, 2016, pp. 7408–7413.

[13] D. Zlotnik, S. Di Cairano, and A. Weiss, "MPC for coupled station keeping, attitude control, and momentum management for GEO satellites using on-off electric propulsion," in *P. IEEE Conf. Contr. Techol. Appl.*, 2017, pp. 1835–1840.

[14] E. M. Soop, *Handbook of Geostationary Orbits*. Springer, 1994.

[15] H. Marquez, *Nonlinear Control Systems*. Hoboken, NJ: John Wiley & Sons, 2003.

[16] A. Weiss, I. Kolmanovsky, D. S. Bernstein, and A. Sanyal, "Inertia-free spacecraft attitude control using reaction wheels," *J. Guid. Control Dynam.*, vol. 36, no. 5, pp. 1425–1439, 2013.

[17] A. Weiss, U. V. Kalabić, and S. Di Cairano, "Station keeping and momentum management of low-thrust satellites using MPC," *Aerosp. Sci. Technol.*, 2018, under review.

[18] A. H. J. de Ruiter, C. J. Damaren, and J. R. Forbes, *Spacecraft Dynamics and Control: An Introduction*. Chichester, West Sussex, UK: John Wiley & Sons, 2013.